High Q-factor near infrared and visible Al 2 O 3 -based parallel-plate capacitor kinetic inductance detectors

Samir Beldi, Faouzi Boussaha, Jie Hu, Alessandro Monfardini, Alessandro Traini, Florence Lévy-Bertrand, Christine Chaumont, Manuel Gonzales, Josiane Firminy, Florent Reix, et al.

Research Article
Vol. 27, No. 9 | 29 Apr 2019 | OPTICS EXPRESS 13319
Optics EXPRESS

High Q-factor near infrared and visible Al_2O_3-based parallel-plate capacitor kinetic inductance detectors

SAMIR BELDI,[1,6] FAOUZI BOUSSAHA,[1,7] JIE HU,[2] ALESSANDRO MONFARDINI,[3] ALESSANDRO TRAINI,[2] FLORENCE LEVY-BERTRAND,[3] CHRISTINE CHAUMONT,[1] MANUEL GONZALES,[5] JOSIANE FIRMINY,[1] FLORENT REIX,[1] MICHAEL ROSTICHER,[4] SHAN MIGNOT,[1] MICHEL PIAT,[2] AND PIERCARLO BONIFACIO[1]

[1]*GEPI, Observatoire de Paris, PSL Université, CNRS, 75014 Paris, France*
[2]*APC, Université de Paris Diderot, 75013 Paris, France*
[3]*Université Grenoble Alpes, CNRS, Grenoble INP, Institut Néel, 38000 Grenoble, France*
[4]*Ecole Normale Supérieure, 45 Rue d'Ulm, 75005 Paris, France*
[5]*Centro Atómico Bariloche, S.C. de Bariloche (8400), Argentina*
[6]*Samir.Beldi@obspm.fr*
[7]*faouzi.boussaha@obspm.fr*

Abstract: We designed, fabricated and characterized parallel-plate capacitor lumped-element kinetic inductance detectors (LEKIDs) to operate at near-infrared and optical wavelengths (0.3 –1 μm). The widely used interdigitated capacitor is replaced by a parallel-plate capacitor which, for a given resonance frequency, has a larger capacitance value within a much smaller space allowing to strongly reduce the size of the pixels. The parallel-plate capacitor LEKID array comprises 10 × 10 pixels. The inductive meander is patterned from stoichiometric 52 nm-thick TiN film (T_c ≈4.6 K). The parallel-plate capacitor is made of a TiN base electrode, Al_2O_3 dielectric and Nb upper electrode. More than 90 resonances out of 100 within the 0.994-1.278 GHz band were identified. The resonances exhibit internal Q-factors up to ~370 000 at 72 mK. The array was illuminated using a white light and 890 nm monochromatic near infrared LEDs. The estimated quasiparticle lifetime is τ_{qp}≈13 μs.

1. Introduction

Over the past 10 years, significant progress has been made in the implementation of visible and near infrared LEKID [1–3] in order to build high-performance instruments for astronomical applications [4,5]. As reported elsewhere [6], the LEKID which typically consists of an interdigitated capacitor shorted by a meandered inductive line, is the most suitable in the visible and near infrared [1,2]. The meander features a unique geometry and it is optimized to act as an efficient photon absorber. The interdigitated capacitor is sized to tune the LEKID resonance frequency within the available band of the readout electronics system. The capacitor size should be large enough to maintain a low resonance frequency, typically a few GHz, which can be easily measured with inexpensive and easy-to-use readout electronics. However, for the classical designs, the interdigitated capacitor can cover up to 90% of the overall pixel surface. This is detrimental for many astrophysical applications as it leads to large pixels and a very low fill factor. The former calls for fast optics to achieve an important transverse magnification or the use of dithering to properly sample the PSF (Point Spread Function) [7] so high spatial resolution can be achieved and strongly limits the number of pixels in the detector. The latter can be partially solved by the introduction of a micro-lens array. Both compromise the performance of visible to near-infrared LEKIDs, which are intrinsically fast and cover a wide wavelength range, and pose optical design challenges for the instrument hosting the detector.

#360592 https://doi.org/10.1364/OE.27.013319
Journal © 2019 Received 20 Feb 2019; revised 4 Apr 2019; accepted 6 Apr 2019; published 25 Apr 2019

Optics EXPRESS

It is hence desirable to reduce the pixel size in LEKIDs typically from hundreds to a few tens of μm.

In this paper, in order to achieve a smaller pixel size, we develop the parallel-plate capacitor LEKID that uses a high dielectric constant material such as Al_2O_3 ($\varepsilon_r \approx 10$) [8]. The parallel-plate capacitor geometry is expected to have another advantage: according to the theoretical model developed by J. Gao et al. [9], it should be possible to increase the detector's sensitivity by reducing the two level systems (TLS) effect usually observed in LEKIDs thanks to the high electric field which can be set inside the parallel-plate capacitor through the power driving the resonators [10]. Indeed, as reported elsewhere [9,11], TLS generate an intrinsic excess noise at the metal/dielectric interface as well as in the bulk substrate that alters the resonance's quality factor and the sensitivity.

2. Design

For comparison, Fig. 1 shows the sketch of the parallel-plate capacitor LEKID along with an interdigitated capacitor LEKID which uses the same meander and is designed to resonate at the same frequency. Thus, the parallel-plate capacitor which features a larger capacitance occupies a much smaller space allowing to reduce the size of pixels.

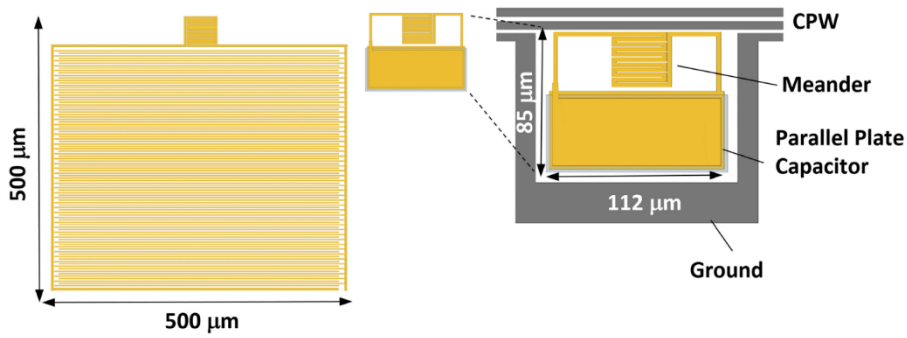

Fig. 1. (Left) Sketch of a classical interdigitated capacitor-based LEKID and (right) our parallel-plate capacitor based LEKID. For comparison, both use the same meander and are designed to resonate at the same frequency of 0.942 GHz. At this frequency, a parallel-plate capacitor LEKID using a 25 nm-thick Al_2O_3 dielectric allows to strongly reduce the size of pixels by a factor 26.

As shown in Fig. 1, LEKID consists of a TiN meandered inductor in parallel with a parallel-plate capacitor, inductively coupled to a 50 Ω CPW feedline. The TiN kinetic inductance per square is calculated using the Mattis-Bardeen relationship $L_k = \hbar \rho/\pi\Delta(T)t$ where $\hbar$ is the reduced Planck constant, t is the thickness, ρ is the resistivity measured before the superconducting transition and $\Delta(T) \approx 1.72 k_B T_c$ is the superconducting energy gap. To achieve best performances, LEKIDs must be cooled below typically $T_c/8$ [12]. At the beginning of this study, because of the limitations of the available fridge which could be cooled down below 300 mK, we chose stoichiometric TiN films of $T_c \sim 4.6$ K with resistivity $\rho \sim 140$ μΩ.cm. These values were extracted using 4-point probe measurements. Thus, a TiN film 52 nm thick yields a sheet kinetic inductance of $L_{k\square} \sim 8$ pH/□. To achieve efficient detection between 0.3 and 1 μm, we set the meander strip width and the gap between strips to respectively $w_m = 2.5$ μm and 0.5 μm [1]. This would lead to a maximum quantum efficiency of about 17% at 380 nm-wavelength as reported by B. Mazin et al. [4]. The meander is connected to the parallel-plate capacitor through two arms. The resonators are designed to resonate within the available readout frequency band of 1-2 GHz. For an inductive strip, including arms, of $l_m = 523$ μm-length, we expect a total kinetic inductance of $L_k = L_{k\square} \times l_m / w_m \approx 1.7$ nH and a geometric inductance [13] of $L_{geo} \approx 0.22$ nH yielding a fractional kinetic inductance of $\alpha_{Tc\approx 4.2K} = L_k/(L_{geo} + L_k) \approx 0.88$. α close to unity guarantees a high sensitivity; hence our interest in an even larger

Optics EXPRESS

kinetic inductance which is achieved at lower critical temperatures (a T_c around 0.8-1 K is usually chosen [1–3]). Another important reason for using large kinetic inductance values is related to the readout frequencies which, according to $f = 1/2\pi(LC)^{0.5}$, should be as low as possible to facilitate the implementation of the readout electronics. Thus, at T_c = 1 K, the calculated sheet kinetic inductance and total kinetic inductance are ~40 pH/□ and ~8.36 nH, respectively, leading to $\alpha_{Tc\approx1K} \approx 0.97$. As demonstrated below, the large capacitance of the dielectric parallel-plate capacitor will offer an opportunity to maintain low readout frequencies despite the use of a rather low value of L_k, with a sensitivity probably lower but still satisfactory as $\alpha_{Tc>1K}$ remains close to unity. Moreover, as stoichiometric TiN's critical temperature would be more homogenous than the sub-stoichiometric [14,15] one over a large substrate area, we expect a more accurate frequency positioning and less frequency collisions.

The parallel-plate capacitor consists of two $L \times w$ = 40 × 100 μm superconducting electrodes separated by a thin Al_2O_3 dielectric layer. To tune the frequency resonance, as shown in Fig. 4, we reduce the upper electrode's area by removing tiles of of $S_N = N \times 4 \times 4$ μm^2 where N is the pixel's number. By comparison, for the interdigitated capacitors, the frequency is usually tuned by changing the length of one or several micro-strips. As a first demonstrator, we devised an array comprising 10 × 10 pixels (i.e., N = 0 to 99). Thus, the value of capacitance can be calculated as follows:

$$C_N = \varepsilon_0 \varepsilon_r (S_F - S_N)/d \tag{1}$$

where $S_F = L \times w$ is the full electrode area and d is the dielectric's thickness. We obtain thus capacitances between 14.16 and 8.55 pF, whereas it is difficult to realize capacitances larger than 1 pF with the classical planar interdigitated capacitor geometry [10]. This yields a capacitance per unit area C_s of 3.54 fF/μm^2 for the parallel-plate capacitor and 0.056 fF/μm^2 for the interdigitated capacitor. Using:

$$f_N = 1/2\pi\sqrt{C_N(L_k + L_{geo})} \tag{2}$$

this results in a readout frequency band of 0.965-1.242 GHz and a frequency spacing Δf_{res} ranging from 1.93 MHz between the first two resonators up to 4.13 MHz between the last two. The frequency resonance spacing is not quite constant as $\Delta f_N \propto 1/(\Delta S_N)^{0.5}$. For the same resonance frequency of around 1 GHz, the parallel-plate capacitor LEKID pixel size is 112 × 85 μm, whereas it is around 500 × 500 μm if the interdigitated capacitor is used while maintaining the same meander.

In order to improve the RF coupling between the resonator and the 50 Ω niobium coplanar waveguide (CPW) feedline, we remove the ground plane on this side of the pixel over its whole length. The meander is 1.5 μm away from the 2 μm-width CPW central line. This does not affect the performance of the feedline as the length of the portion removed is much smaller than the RF readout's wavelength. In addition, the arms which are defined along the central line at the same distance (i.e., 1.5 μm), replace almost entirely the removed ground, thus contributing to optimizing the RF coupling between the feedline and the pixel as shown by the simulations in Fig. 2. They show the simulated forward transmission S_{21} response of the feedline as well as the current density within the parallel-plate capacitor LEKID with a full upper electrode using the electromagnetic simulation package SONNET [16]. The simulated internal and coupling quality factors are $Q_i \approx 600\,000$ and $Q_c \approx 40\,000$, respectively. As calculated using Eq. (2), it resonates at 0.946 GHz which is the lowest frequency of the array. The current distribution shows that the coupling is done thanks to the meander and arms.

Optics EXPRESS

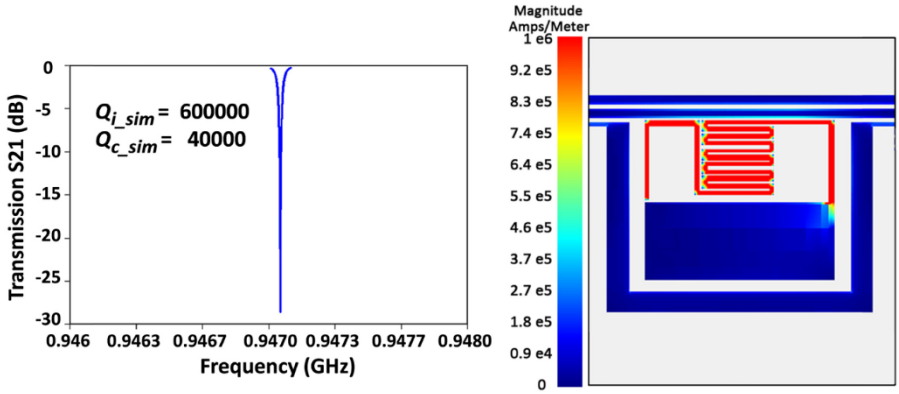

Fig. 2. SONNET simulation of a parallel-plate capacitor based LEKID with a full upper electrode. The left panel presents the forward transmission (S21) signal of the 50 Ω feedline showing the LEKID resonance at 0.947 GHz. The right panel shows the current density within the meander along with the parallel-plate capacitor. The current is almost entirely confined in the meander.

3. Fabrication

The sketch in Fig. 3 depicts our sequence of the fabrication of LEKIDs which use sputter deposition, 320 and 360 nm UV lithography as well as lift-off techniques.

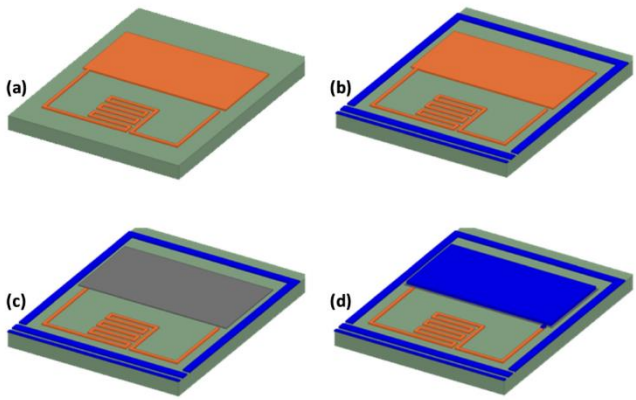

Fig. 3. LEKID fabrication sequence which consists in (a) TiN meander and bottom electrode deposition. The TiN layer is deposited at a rate ~1 nm/s using Ar and N_2 flow rates of respectively 50 sccm and 6 sccm at a total pressure of 0.6 Pa with a 700 W DC power. These deposition conditions lead to a desired T_c of ~4.6 K. (b) Nb feedline and ground plane deposition. The Nb layer is deposited using a 50 sccm Ar flow rate, 1.1 Pa total pressure and 500 W DC power. (c) Al_2O_3 dielectric deposition using an atomic layer deposition technique. (d) Nb top electrode deposition using the same parameters as for the CPW feedline. Before each deposition, the substrate is cleaned for 2 min with a 50 sccm Ar flow rate, 1.1 Pa total pressure and 50 W RF power. TiN and Nb are deposited in a sputtering system equipped with a high vacuum load-lock and 6-inch (Ti, Nb) targets. A base pressure of ~2.8×10^{-8} mbar is reached before deposition. The substrate is positioned at 80 mm from the target.

All the superconducting layer/silicon substrate depositions are done with a background pressure below 3×10^{-8} mbar. Interface is crucial to achieving high quality resonances, we paid particular attention to substrate cleaning. We used 50 mm diameter and 280 µm-thick high resistivity silicon substrate (>15 kΩ.cm) cleaned using a process based on hydrofluoric acid (HF). The fabrication process starts with the patterns of TiN 52 nm-thick inductive meanders, for the lower rectangular electrodes followed by those of the niobium (Nb) 100 nm-thick CPW

feedline. Compared to TiN, Nb has a lower surface impedance making it easier to build the 50 Ω feedline [1]. The use of 320 nm UV allowed us to easily achieve 0.5 µm spacing within the meander. The 52 ± 2 nm-thick TiN layer is deposited at a rate ~1 nm/s using Ar and N_2 flow rates of respectively 50 and 6 sccm at a total pressure of 0.6 Pa with a 700 W DC power. These deposition conditions lead to the desired T_c of ~4.6 K (i.e stoichiometric TiN layer). The niobium is deposited using a 50 sccm Ar flow rate, 1.1 Pa total pressure and 500 W DC power. The 25 ± 1 nm-thick Al_2O_3 layer is then deposited using ALD technique (Atomic Layer Deposition) at a rate of 0.166 nm/min allowing to achieve a compact and thin layer with a high accuracy on the thickness. During the deposition, the temperature of the substrate is raised to 175°C. The Al_2O_3 layer is then patterned into rectangular panels by optical lithography followed by a wet etching process. Finally, the 100 nm-thick Nb upper electrode is deposited using the same parameters as the CPW feedline. Note that, right before each deposition, the substrate is cleaned with RF argon plasma in the sputtering machine. This is particularly important to ensure, on the one hand, the cleanest base electrode surface before the dielectric deposition and, on the other hand, the best electrical contact between meanders and upper electrodes.

4. Experimental results

4.1 Resonances in dark

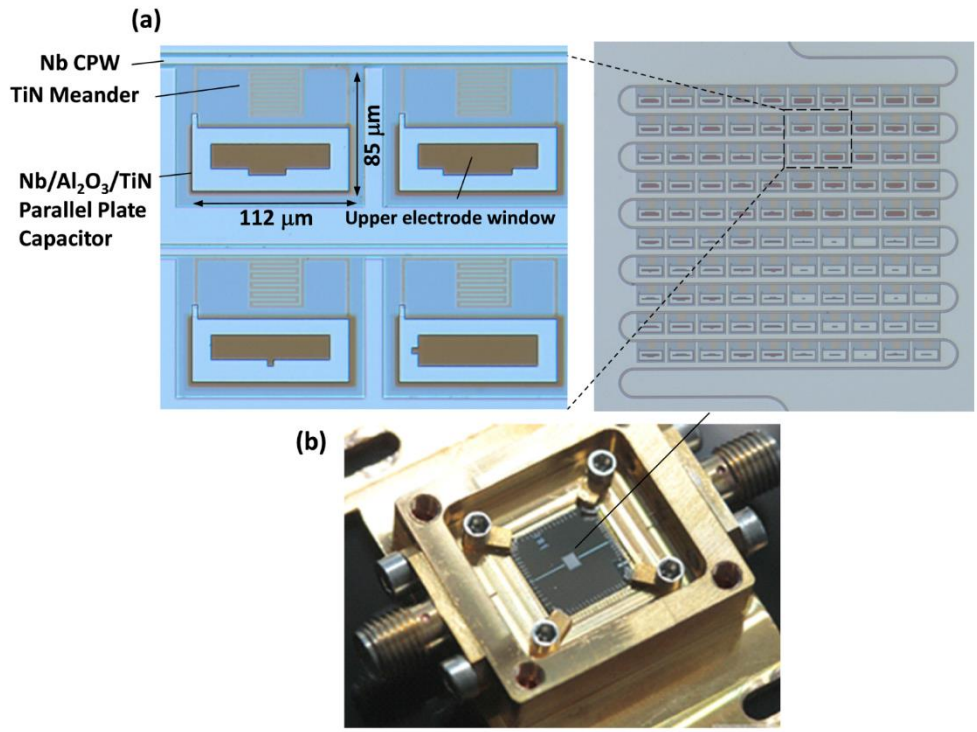

Fig. 4.(a) Optical microscope picture of the 10 × 10 pixel array and zoom-in picture of four pixels. Upper electrodes feature different window sizes to tune the resonance frequency. (b) Parallel-plate capacitor array mounted in a gold-plated copper box and wire-bonded to two 50 Ω SMA connectors.

Figure. 4 shows the fabricated 100-pixel array which is mounted and Al-wire-bonded to two 50 Ω SMA connectors in a gold-plated copper box and cooled down to 300 and 72 mK by means of two different fridges. The 300 mK fridge which is equipped with a LED is used to illuminate the array and perform the first photometric measurements. The 72 mK fridge is used

Optics EXPRESS

to estimate quality factors as a function of the feedline power. The resonance patterns are recorded using a vector network analyzer. Figure 5 shows the forward transmission of the feedline where 96 resonances out of 100 were observed within a 284 MHz bandwidth between 0.994 and 1.278 GHz at 72 mK. The band is very close to the one calculated and simulated. Furthermore, the resonances are distributed almost as expected over the fixed readout bandwidth. As designed, we can note a tight frequency spacing Δf_{res} at the lower end of the band which progressively widens towards the upper end. We measured an average Δf_{res} of ~2 MHz for the first ten resonances and ~5 MHz for the last ten. We also observed only 5 frequency overlaps. These results demonstrate that uncertainties on and dispersion of fabrication parameters values, with respect to the design are small and well controlled, particularly concerning the Al_2O_3 and TiN layers. As shown by the histograms in Fig. 6, the internal quality factors range from Q_{i_min} ~4×10^4 to Q_{i_max} ~2.8×10^5 with an average of Q_i ~1.6×10^5 when a power on the feedline of −100 dBm is applied. This translates into a loss tangent $\tan \delta_i = 1/Q_i$ between ~2.5×10^{-5} and ~3.7×10^{-6} with an average of ~6.6×10^{-6}. The measured coupling factors are between Q_{c_min} ~9.4×10^3 and Q_{c_max} ~6.6×10^4 with an average of Q_c ~2.8×10^4. The total quality factor is $Q_T = 1/(Q_i^{-1} + Q_c^{-1})$ ≈2.38×10^4 approaching Q_c.

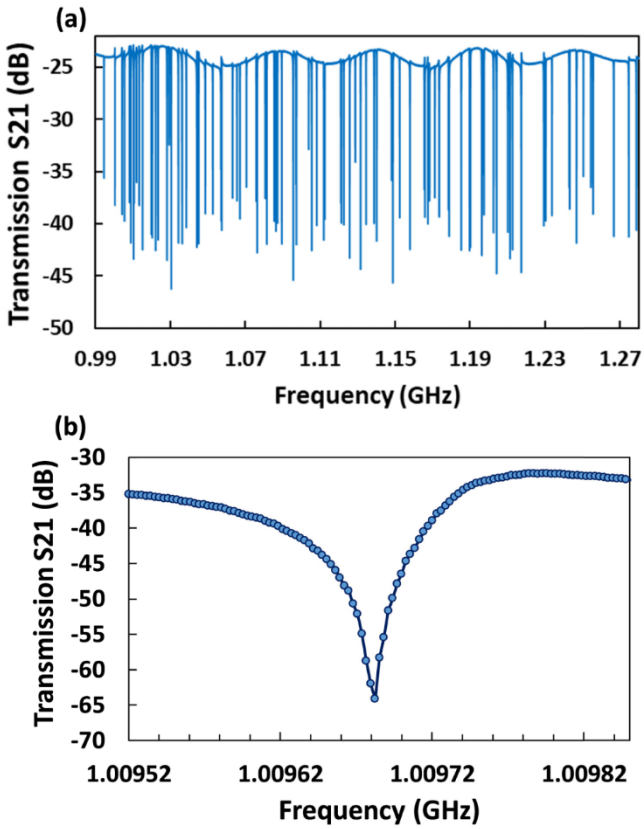

Fig. 5. (a) Forward transmission S_{21} of the CPW feedline showing 96 resonances out of 100 at 72 mK measured with a power on the feedline of P_f = 105 dBm. (b) Isolated resonance at f_0 ≈1.009 GHz with Q_{i_max} ≈378 000 when a feedline power of P_f = –90 dBm is applied.

These results approach those achieved with dielectrics known to be low loss such as the single crystal silicon [17] and amorphous hydrogenated silicon nitride (a-SiN_x:H) [18] or even vacuum parallel-plate capacitor [19]. Moreover, similar results are obtained with optical planar interdigitated capacitor LEKIDs we made using the same fabrication process. At a lower

Optics EXPRESS

feedline power of −110 dBm, the average Q_i decreases down to ~0.94 × 10^5 whereas it increases up to ~2.1 × 10^5 at a higher power of −90 dBm. As reported by G. Coiffard et al. [10], the improvement of the quality factor with the feedline power is probably due to the higher electrical field between the capacitor plates reducing TLS by saturation. However, further investigation is needed to quantify the feedline power dependence of Q_i in the parallel-plate capacitor compared to the interdigitated geometry.

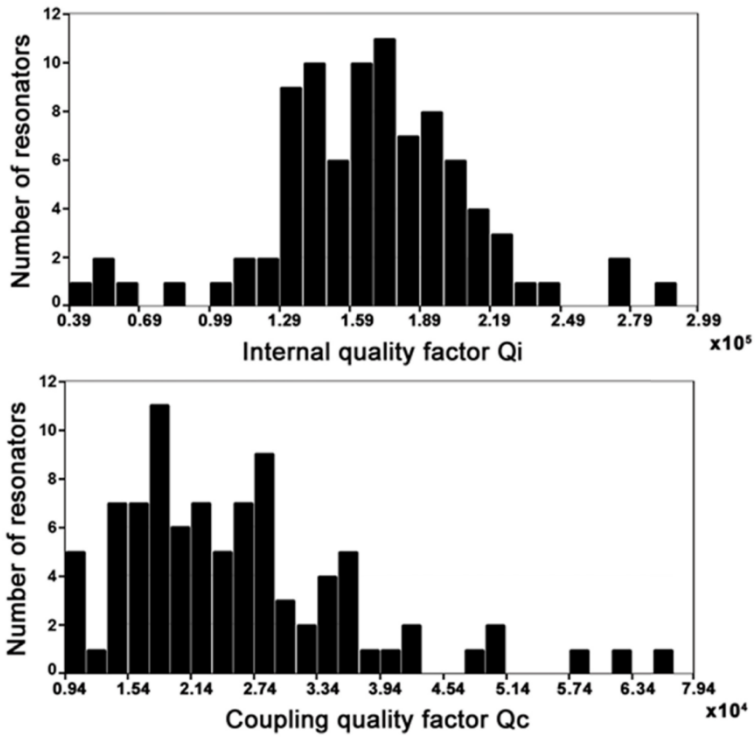

Fig. 6. Histograms of internal Q_i (top) and coupling Q_c (bottom) quality factors for 91 resonators out of 100. Q_i and Q_c are obtained by fitting the resonance plots. The power on the feedline is P_f = −100 dBm.

4.2 Illuminated resonances

To assess whether our LEKIDs can detect near infrared and visible photons, we illuminated the array using a 890 nm monochromatic near infrared and a white light LEDs in the 300 mK fridge. No lens was used. The LEDs were placed at a distance of 10 mm from the array on the 300 mK stage. As shown in Fig. 7(b), switching on the monochromatic LED causes a shift towards lower frequencies as well as a reduction in depth of all the observed resonances. The same behavior is observed with the visible LED. The arrival of a photon on a given pixel can be detected by this change in frequency and depth of the resonance. Since, we do not have access to the calibrated LED radiant powers at such a low temperature, these measurements are qualitative and did not allow us to deduce noise equivalent power (NEP) which should be done in a cryostat equipped with an optical fiber. We also estimated the quasi-particle lifetime τ_{qp} using an experimental setup shown in Fig. 7(a) based on homodyne detection [20]. The quasiparticle lifetime is estimated by probing the transmission signal phase in the time domain when the array is illuminated by the monochromatic LED which is modulated by a 1 kHz pulse with 1μs width generated by a pulse generator. As shown in Fig. 7(c), the estimated quasiparticle lifetime is τ_{qp} ≈13 μs which is consistent with experimental results reported

Optics EXPRESS

elsewhere [21] using interdigitated capacitor LEKIDs with stoichiometric TiN. Longer lifetimes are expected using sub-stoichiometric TiN films (T_c~1K).

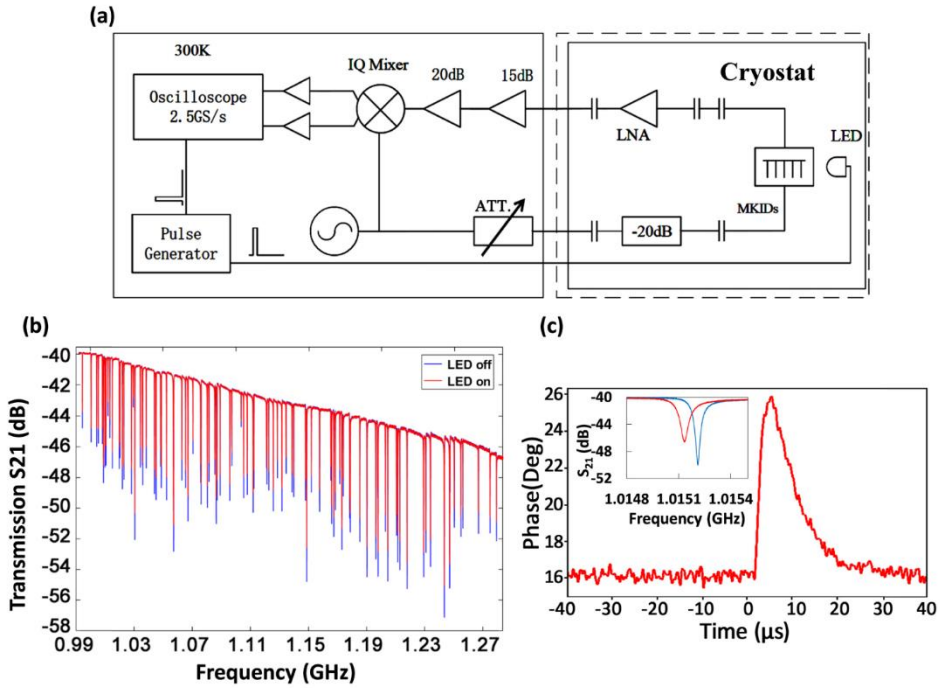

Fig. 7. (a) Layout of the cryogenic test bench used to estimate the quasiparticule lifetime with our parallel-plate capacitor LEKIDs. It operates as follows: a 17 dBm signal generated by a local oscillator (LO) is attenuated to −80 dBm using a voltage-controlled attenuator and a −20 dB attenuator before reaching the LEKIDs into the 300 mK fridge. The signal modified by the resonators is then amplified by a 30 dB-gain cryogenic low noise amplifier (a Narda-MITEQ amplifier) and two room temperature amplifiers that feature a total gain of 35 dB. The amplified signal is then mixed with the reference signal (the LO signal) and down converted to a DC signal by an IQ Mixer in order to extract the amplitude and phase. These two components are amplified then digitalized by an oscilloscope at a 2.5 GSPS/s sample rate. (b) All resonances illuminated with a 890 nm monochromatic LED at 320 mK when a feedline power of around −80 dBm is applied. At this temperature, the average internal quality factors decrease to ~8.7×10^4 with a maximum of ~1×10^5. The slope is due to the readout system. (c) Quasiparticle lifetime estimate. The inset shows one of the resonances (f_0 = 1.0152GHz, Q_i ≈50 000, Q_c ≈17 400) when the array is illuminated by the 890 nm monochromatic LED leading to a frequency shift up to Δf_0 ≈100 kHz. The low Q_i compared to the average value at 320 mK is due to the high power (around −80 dBm) on the feedline.

5. Conclusion

In conclusion, we demonstrated the technology to build arrays of Al_2O_3-based parallel-plate capacitor LEKIDs. The resonators which were successfully frequency multiplexed thanks to the change of the upper electrode area, featured high quality factors (>10^5). We think that this is probably due, on the one hand, to the low amount of defects in the Al_2O_3 layer deposited by atomic layer deposition, and on the other hand, to a weaker TLS noise saturated by the high power applied on the feedline. For a given frequency readout bandwidth, compared to the interdigitated capacitor geometry, the use of the parallel-plate capacitor allows to significantly reduce the size of optical LEKIDs resonating at rather low frequencies (~1-1.3 GHz). Perspectives include, the use of sub-stoichiometric TiN with a lower T_c (~1 K instead of 4.6 K), and thus a larger kinetic inductance which will yield lower resonant frequencies (<1GHz) with better performance, particularly in terms of sensitivity. This will significantly facilitate

the implementation of the readout electronics. Beyond astronomy, the low loss Al_2O_3-based superconducting resonators achievement would also be great interest to other superconducting circuits such as quantum bits [22] and quantum memories.

Funding

l'Ecole Doctorale d'Astronomie et d'Astrophysique d'Ile de France (ED127) and PSL-Paris Observatory.

Acknowledgments

We thank Jean-Pierre Aoustin and Laurent Pelay for copper box fabrication, José Palamo for Al_2O_3 deposition and Martino Calvo for support during the measurements. We acknowledge Pascal Jagourel for his continued support. The devices were fabricated in Paris Observatory clean-room facility and characterized at AstroParticle and Cosmology (APC) Lab as well as at CNRS-Néel Institute.

References

1. B. A. Mazin, B. Bumble, S. R. Meeker, K. O'Brien, S. McHugh, and E. Langman, "A superconducting focal plane array for ultraviolet, optical, and near-infrared astrophysics," Opt. Express **20**(2), 1503–1511 (2012).
2. P. Szypryt, S. R. Meeker, G. Coiffard, N. Fruitwala, B. Bumble, G. Ulbricht, A. B. Walter, M. Daal, C. Bockstiegel, G. Collura, N. Zobrist, I. Lipartito, and B. A. Mazin, "Large-format platinum silicide microwave kinetic inductance detectors for optical to near-IR astronomy," Opt. Express **25**(21), 25894–25909 (2017).
3. P. Szypryt, B. A. Mazin, G. Ulbricht, B. Bumble, S. R. Meeker, C. Bockstiegel, and A. B. Walter, "High quality factor platinum silicide microwave kinetic inductance detectors," Appl. Phys. Lett. **109**(15), 151102 (2016).
4. B. A. Mazin, S. R. Meeker, M. J. Strader, P. Szypryt, D. Marsden, J. C. V. Eyken, G. E. Duggan, A. B. Walter, G. Ulbricht, and M. Johnson, "ARCONS: A 2024 pixel optical through near-IR cryogenic imaging spectrophotometer," Pub Astronomical Soc. Pacific **125**, 1348–1361 (2013).
5. S. R. Meeker, B. A. Mazin, A. B. Walter, P. Strader, N. Fruitwala, C. Bockstiegel, P. Szypryt, G. Ulbricht, G. Coiffard, B. Bumble, G. Cancelo, T. Zmuda, K. Treptow, N. Wilcer, G. Collura, R. Dodkins, I. Lipartito, N. Zobrist, M. Bottom, J. C. Shelton, D. Mawet, J. C. van Eyken, G. Vasisht, and E. Serabyn, "DARKNESS: a microwave kinetic inductance detector integral field spectrograph for high-contrast astronomy," Astronomical Soc. Pacific **130**(988), 065001 (2018).
6. S. Doyle, P. Mauskopf, J. Naylon, A. Porch, and C. Duncombe, "Lumped element kinetic inductance detectors," J. Low Temp. Phys. **151**(1-2), 530–536 (2008).
7. T. R. Lauer, "The photometry of undersampled point-spread functions," Astronomical Soc. Pacific. **111**(765), 1434–1443 (1999).
8. S. Beldi, F. Boussaha, C. Chaumont, S. Mignot, F. Reix, A. Tartari, T. Vacelet, A. Traini, M. Piat, and P. Bonifacio, "Design of near infrared and visible kinetic inductance detectors using MIM capacitors," J. Low Temp. Phys. **193**(3-4), 184–188 (2018).
9. J. Gao, M. Daal, A. Vayonakis, S. Kumar, J. Zmuidzinas, B. Sadoulet, B. A. Mazin, P. K. Day, and H. G. Leduc, "Experimental evidence for a surface distribution of two-level systems in superconducting lithographed microwave resonators," Appl. Phys. Lett. **92**(15), 152505 (2008).
10. G. Coiffard, B.Mazin, Paul Szypryt, G. Ulbricht, M. Daaland, and N. Zobris, "Parallel plate microwave kinetic inductance detectors," Low Temperature Detectors (LTD) workshop, Japan, July (2017).
11. O. Noroozian, J. Gao, J. Zmuidzinas, H. G. LeDuc, B. A. Mazin, B. Young, B. Cabrera, and A. Miller, "Two-level system noise reduction for microwave kinetic inductance detectors," AIP Conf. Proc. **1185**, 148–151 (2009).
12. P. Szypryt, "Development of Microwave Kinetic Inductance Detectors for Applications in Optical to Near-IR Astronomy," PhD dissertation, University of California - Santa Barbara (2017).
13. S. Doyle, "Lumped Element Kinetic Inductance Detectors," PhD dissertation, Cardiff University (2008).
14. G. Coiffard, K. F. Schuster, E. F. C. Driessen, S. Pignard, M. Calvo, A. Catalano, J. Goupy, and A. Monfardini, "Uniform non-stoichiometric titanium nitride thin films for improved kinetic inductance detector arrays," J. Low Temp. Phys. **184**(3-4), 654–660 (2016).
15. M. R. Vissers, J. Gao, J. S. Kline, M. Sandberg, M. P. Weides, D. S. Wisbey, and D. P. Pappas, "Characterization and in-situ monitoring of sub-stoichiometric adjustable superconducting critical temperature titanium nitride growth," Thin Solid Films **548**, 485–488 (2013).
16. http://www.sonnetsoftware.com/
17. S. J. Weber, K. W. Murch, D. H. Slichter, R. Vijay, and I. Siddiqi, "Single crystal silicon capacitors with low microwave loss in the single photon regime," Appl. Phys. Lett. **98**(17), 172510 (2011).
18. H. Paik and K. D. Osborn, "Reducing quantum-regime dielectric loss of silicon nitride for superconducting quantum circuits," Appl. Phys. Lett. **96**(7), 072505 (2010).

Optics EXPRESS

19. K. Cicak, D. Li, J. A. Strong, M. S. Allman, F. Altomare, A. J. Sirois, J. D. Whittaker, J. D. Teufel, and R. W. Simmonds, "Low-loss superconducting resonant circuits using vacuum-gap-based microwave components," Appl. Phys. Lett. **96**(9), 093502 (2010).
20. P. K. Day, H. G. LeDuc, B. A. Mazin, A. Vayonakis, and J. Zmuidzinas, "A broadband superconducting detector suitable for use in large arrays," Nature **425**(6960), 817–821 (2003).
21. H. G. Leduc, B. Bumble, P. K. Day, B. H. Eom, J. Gao, S. Golwala, B. A. Mazin, S. McHugh, A. Merrill, D. C. Moore, O. Noroozian, A. D. Turner, and J. Zmuidzinas, "Tianium nitride films for ultrasensitive microresonator detectors," Appl. Phys. Lett. **97**(10), 102509 (2010).
22. J. M. Martinis, K. B. Cooper, R. McDermott, M. Steffen, M. Ansmann, K. D. Osborn, K. Cicak, S. Oh, D. P. Pappas, R. W. Simmonds, and C. C. Yu, "Decoherence in Josephson qubits from dielectric loss," Phys. Rev. Lett. **95**(21), 210503 (2005).